Headpiece domain of dematin is required for the stability of the erythrocyte membrane

Richie Khanna*, Seon H. Chang†, Shaida Andrabi*, Mohammad Azam*, Anthony Kim*, Alicia Rivera‡, Carlo Brugnara‡, Philip S. Low†, Shih-Chun Liu*, and Athar H. Chishti*§

*Departments of Medicine, Anatomy, and Cellular Biology, St. Elizabeth's Medical Center, Tufts University School of Medicine, Boston, MA 02135; †Department of Chemistry, Purdue University, West Lafayette, IN 47907-1393; and ‡Department of Laboratory Medicine, Children's Hospital, Harvard Medical School, Boston, MA 02115

Communicated by Daniel Branton, Harvard University, Cambridge, MA, March 15, 2002 (received for review January 6, 2002)

Dematin is an actin-binding and bundling protein of the erythrocyte membrane skeleton. Dematin is localized to the spectrin–actin junctions, and its actin-bundling activity is regulated by phosphorylation of cAMP-dependent protein kinase. The carboxyl terminus of dematin is homologous to the "headpiece" domain of villin, an actin-bundling protein of the microvillus cytoskeleton. The headpiece domain contains an actin-binding site, a cAMP-kinase phosphorylation site, plays an essential role in dematin self-assembly, and bundles F-actin *in vitro*. By using homologous recombination in mouse embryonic stem cells, the headpiece domain of dematin was deleted to evaluate its function *in vivo*. Dematin headpiece null mice were viable and born at the expected Mendelian ratio. Hematological evaluation revealed evidence of compensated anemia and spherocytosis in the dematin headpiece null mice. The headpiece null erythrocytes were osmotically fragile, and ektacytometry/micropore filtration measurements demonstrated reduced deformability and filterability. *In vitro* membrane stability measurements indicated significantly greater membrane fragmentation of the dematin headpiece null erythrocytes. Finally, biochemical characterization, including the vesicle/cytoskeleton dissociation, spectrin self-association, and chemical crosslinking measurements, revealed a weakened membrane skeleton evidenced by reduced association of spectrin and actin to the plasma membrane. Together, these results provide evidence for the physiological significance of dematin and demonstrate a role for the headpiece domain in the maintenance of structural integrity and mechanical properties of erythrocytes *in vivo*.

The membrane bilayer and the network of membrane-associated proteins together regulate the characteristic shape and elastic properties of red blood cells (1, 2). When membrane skeletons are prepared in the presence of a high concentration of monovalent salt, the core of the membrane skeleton consists of spectrin, actin, protein 4.1, and dematin (3). Although the functions of spectrin, actin, and protein 4.1 have been extensively characterized (4, 5), virtually nothing is known about the physiological function in mature erythrocytes of dematin, a three-subunit protein that migrates in the protein 4.9 region during electrophoresis. The earliest evidence suggesting a membrane stabilizing role for dematin came from Holdstock and Ralston (6). They demonstrated that charged sulfhydryl compounds such as *p*-chloromercuribenzene sulfonateS preferentially attach to dematin and cause the disruption of erythrocyte cytoskeletons. Dematin is a substrate for multiple protein kinases, and phosphorylation of dematin by the cAMP-dependent protein kinase is known to regulate dematin's actin-bundling activity *in vitro* (7–9). The major phosphorylation site of the cAMP-dependent protein kinase is located within the headpiece domain of dematin (10), but the physiological significance of dematin phosphorylation is not known.

Siegel and Branton (11) conducted the first systematic functional characterization of dematin by demonstrating its actin bundling activity *in vitro*. Because actin bundles appear to be absent in mature erythrocytes, dematin's role in actin bundling events remains unclear. Therefore, dematin's physiological function might be accounted for by its actin-binding activity or by as yet unknown binding functions in the mature erythrocytes. In this context, dematin's stoichiometry in human erythrocytes is significant. A quantitative ELISA revealed ≈43,000 copies of trimeric dematin (8, 9). Because there are 500,000 actin monomers per human erythrocyte, and 12–13 monomers in each actin oligomer (12, 13), there must be about ≈40,000 actin oligomers per erythrocyte. It is therefore likely that one dematin trimer is associated with one actin oligomer *in vivo*. Dematin is a trimeric assembly of two 48-kDa polypeptides and one 52-kDa polypeptide (10). The C-terminal 75 residues of both polypeptides are homologous to the headpiece domain of villin, an actin-binding protein of the brush border cytoskeleton (14). Here, we have used gene-targeting techniques to delete the headpiece domains of both the 48-kDa and the 52-kDa subunits of mouse dematin and demonstrate their functional requirement in the maintenance of erythrocyte shape and membrane mechanical properties *in vivo*.

BIOCHEMISTRY

Materials and Methods

Targeted Deletion of the Headpiece Domain. A mouse P1 genomic library (Genome Systems, St. Louis) was screened by using primers 5′-ATGGAACGGCTGCAGAAG and 3′-GTTCTTCTTCCGGAGAGAGAA derived from human dematin coding sequence. Two clones, designated as P1#7227 and P1#7228, were isolated that contained the entire dematin gene as determined by Southern blot analysis. The headpiece domain of dematin is encoded by exons 10–15 (15, 16). An upstream arm of 8 kb encoding exons 9–10 and a downstream arm of 1.2 kb extending beyond exon 15 were cloned into the vector pPNT, thus flanking the neomycin resistance gene. This targeting vector was linearized by *Sfi*I, and ≈20 μg of linearized vector was electroporated into ES cells (129/SVJ mouse AK7-cells) by using a Bio-Rad gene pulser at 0.25 V and 960 μF. Cells were plated on feeder layers in normal growth medium for 36–48 h, followed by selection with 175 μg/ml G418. After 8–10 days, G418 colonies were picked up and screened by Southern blot hybridization for correct targeting. The correctly targeted ES clones were injected into the blastocysts from C57BL/6J mice, which were transferred to the uteri of pseudopregnant recipients. Male chimeras were bred with C57BL/6J female mice, and tail DNA from agouti F_1 offspring was genotyped by Southern blot. F_1 heterozygous females and F_1 wild-type males were interbred, and the littermates were genotyped by PCR. PCR was carried out by using forward primer MD43 (5′-CCTTGCATTCGGGAACATCTAAATC) from exon 10 and reverse primer MD32 (5′-GGTACTGTCACGGACAGGGCGAGC) located downstream of exon 15. The PCR products were 1.3 kb and 1.7 kb from wild-type and mutant mice, respectively.

Abbreviations: ES, embryonic stem; HPKO, headpiece knock out; RT, reverse transcription; DI, deformability index; IOV, inside-out vesicle; m.w., molecular weight.

§To whom reprint requests should be addressed. E-mail: athar.chishti@tufts.edu.

The publication costs of this article were defrayed in part by page charge payment. This article must therefore be hereby marked "*advertisement*" in accordance with 18 U.S.C. §1734 solely to indicate this fact.

Immunoblotting and Reverse Transcription (RT)-PCR. Ghosts were prepared from an equal number of RBCs obtained from wild-type and homozygous mice. Ghost proteins were separated by SDS/PAGE (10% gel) and Western blotted by using a monoclonal antibody raised against the core domain of human dematin (1:10,000 dilution). Dematin monoclonal antibody recognizes an epitope located between amino acids 68–190 of the core domain (Transduction Laboratories, Lexington, KY). Dematin transcripts in the brain and kidney tissues were analyzed by RT-PCR. Reverse transcribed cDNA was amplified by using forward primer MD43 and reverse primer MD32, using One Step RT-PCR Kit (CLONTECH Advantage One Step RT-PCR Kit).

Hematological Analysis. Blood from wild-type and dematin headpiece knock out (HPKO) mice was collected in the sodium-heparin tubes. An aliquot of blood (50 μl) was used to measure the red cell indexes [hematocrit, mean corpuscular volume (MCV), mean cell hemoglobin concentration (MCHC), hemoglobin, and reticulocyte number] by using a hemoanalyzer (ADVIA 120; Bayer, Elkhart, IN) with software designed for murine hematology.

Microscopy. Peripheral blood was obtained from wild-type and dematin HPKO mice and washed once with PBS. Morphology of unfixed RBCs was examined by phase contrast microscopy. For scanning electron microscopy, washed RBCs were fixed in 0.25% glutaraldehyde (freshly prepared in PBS) for 2 h at 0°C. Fixed cells were dehydrated in different grades of alcohol and subjected to critical point drying. Samples were coated with a thin layer of carbon on critical point drying (CPD) grids, and visualized by the scanning electron microscope (Tufts University EM Facility).

Osmotic Fragility Assay. Osmotic fragility of erythrocytes was measured on freshly collected blood in heparin from ≈8-mo-old mice. RBCs were washed with the isotonic saline and suspended in varying concentrations of NaCl. Samples were incubated at room temperature for 30 min and centrifuged at 1,500 × *g* for 10 min at 4°C. The supernatant was collected, and absorbance was measured at 540 nm with appropriate controls. The percentage lysis of RBCs was calculated from the absorbance, and a fragility curve was generated by plotting varying salt concentrations vs. hemolysis.

Osmotic Deformability and Membrane Stability Measurements. Freshly isolated packed RBCs were suspended in 4% polyvinylpyrrolidone [molecular weight (m.w.) 360,000] in PBS and examined by ektacytometry, a laser diffraction method described elsewhere (17, 18). For osmotic gradient ektacytometry, suspended erythrocytes were subjected to increasing osmolality (from 50–500 mosM/kg) at constant shear stress and the axial ratio of the deformed cells was quantified by laser diffraction and designated as their deformability index (DI). Measurements of DI as a function of osmolality and shear stress can provide information on the hydration of the cell. For measurement of membrane stability, packed RBCs were lysed in 40 vol of 10 mM sodium phosphate (pH 7.4) and pelleted at 20,000 × *g*. After centrifugation, the lysed erythrocytes were resealed by adding 20 vol of PBS and incubating for 45 min at 37°C. The resealed ghosts were washed once with PBS, resuspended in 35% dextran-phosphate buffer, and analyzed by ektacytometry at a constant high applied shear stress (785 dynes/cm^2), as described above. The decline in deformability with time derives from mechanical fragmentation of the membranes into nondeformable vesicles. The half time for this shear-induced fragmentation can be used as a measure of the membrane's mechanical stability (19).

Erythrocyte Filterability Assay. Analysis of the rate of filtration of an RBC suspension through a highly uniform, laser-crafted nickel mesh filter was conducted by a gravity-based, vertical tube method (20) that measures the rate of passage of erythrocytes through the filter as a function of hydrostatic pressure (Tsukusa Sokken, Tokyo). The pore diameter of the nickel mesh used in this study was 4.6 microns. For a height (pressure)-time curve obtained during the filtration analysis, a pressure-flow rate relationship can be determined. The filtration was initiated at a pressure of 150 mm H_2O, and the flow rate (ml/min) of the RBC suspension (0.1% hematocrit) relative to that of the suspending medium at 100 mm H_2O was taken as the index of RBC filterability.

Biochemical Characterization. Triton shells were prepared by solubilizing RBC ghosts in 1% Triton X-100 solution containing 50 mM Tris·HCl (pH 7.5), 1 mM EDTA, 1 mM EGTA, and 1 mM PMSF with varying KCl concentrations. After incubation on ice for 60 min, samples were centrifuged at 55,000 × *g* for 60 min at 4°C, and pellets were analyzed by 10% SDS/PAGE. Inside-out vesicles (IOVs) were prepared by washing RBC ghosts with the low ionic strength buffer (0.1 mM phosphate buffer, pH 8.0/0.1 mM EDTA/0.1 mM PMSF/0.1 mM DTT) at 4°C. Washed ghosts (1 vol) were mixed thoroughly with 3 vol of the same buffer and incubated at 0°C for ≈12 h. Samples were centrifuged at 55,000 × *g* for 60 min at 4°C to collect IOVs. Spectrin tetramers were isolated by incubation of RBC ghosts in low ionic strength buffer at 0°C for 48 h. Samples were centrifuged at 55,000 × *g* for 120 min at 4°C. Supernatant was immediately reconstituted to a final concentration of 40 mM Tris·HCl (pH 7.4), 20 mM sodium acetate, 2 mM DTT, and 2 mM EDTA, and spectrin self-association was analyzed by nondenaturing polyacrylamide gel electrophoresis (4% gel) at 4°C for 48 h (21).

Chemical crosslinking was performed by incubating 1 vol of packed RBC ghosts (minus EDTA) with 30 vol of oxidizing agent consisting of $CuSO_4$ (10 μM) and *O*-phenanthroline (50 μM; ref. 11). Samples were incubated at room temperature for 60 min, and crosslinking reaction was terminated by the addition of 2 mM EDTA. Membrane pellet was solubilized in the electrophoresis buffer without reducing power for 30 min at 37°C and analyzed by Fairbanks SDS/PAGE (5.6% gel) without DTT (22). One portion of the gel was stained with Coomassie blue, and the other half was processed for Western blotting.

Results

Targeted Deletion of the Headpiece Domain of Dematin. Because the headpiece domain confers *in vitro* functionalities to dematin, its deletion was expected to provide a clue to the physiological function(s) of dematin *in vivo*. Homologous recombination in ES cells was used to selectively delete the headpiece domain of mouse dematin. The targeted pPNT vector contains the neomycin resistance gene inserted immediately after exon 10, thus deleting exons 11–15 encoding the headpiece domain of dematin (Fig. 1*A*). Disruption of the dematin allele in ES cells was confirmed by Southern blot hybridization (Fig. 1*B*). Wild-type ES cells (+/+) revealed an expected 3.6-kb *Nco*I fragment whereas the targeted ES cells (+/−) show two fragments of 3.6 kb and 2.0 kb, respectively (Fig. 1*B*). The 2.0-kb targeted fragment originates from an internal *Nco*I site within the neomycin resistance gene. One of the positive ES clones was injected into blastocysts to generate chimeric mice, which were mated to generate heterozygous and homozygous animals. Wild-type, heterozygous, and homozygous progeny were obtained in a typical Mendelian ratio of 1:2:1, and typed by PCR using primers specific for the headpiece domain of dematin (Fig. 1*C*). As expected, a single band of 1.3 kb in the wild type (+/+), two bands of 1.3 kb and 1.7 kb in the heterozygous, and a single band of 1.7 kb in the homozygous mice (−/−) were detected (Fig. 1*C*). These results demonstrate correct targeting of the engineered vector at the dematin locus in the mouse genome.

To ensure systemic deletion of the headpiece domain, we used RT-PCR to detect dematin transcripts in the kidney and brain tissues where dematin is abundantly expressed (23). Indeed, no signal was detected in the homozygous mice (Fig. 1*D*), indicating that we have generated genetically altered mice selectively lacking the headpiece domain of dematin. Dematin was originally discovered in mature erythrocytes where its presence continues to remain enigmatic, mainly because of the apparent lack of actin bundles in

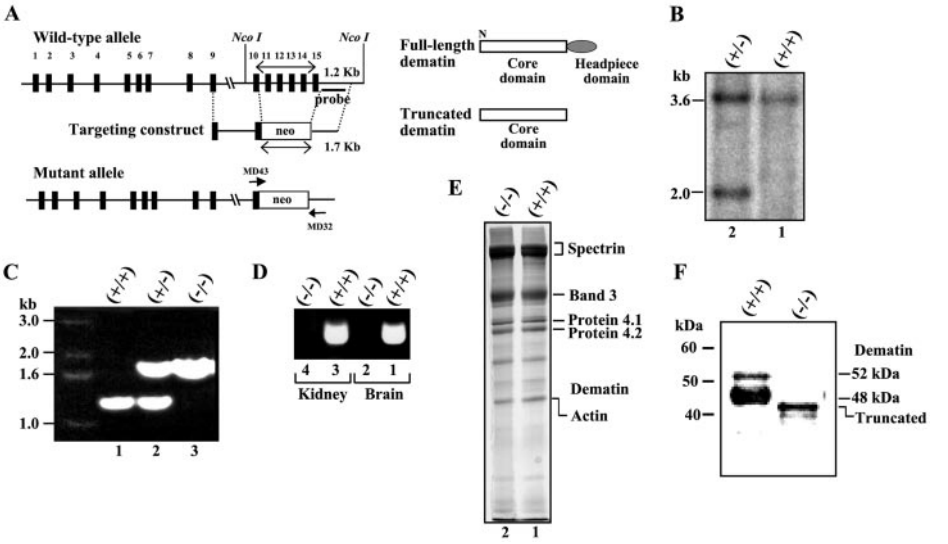

Fig. 1. Targeted deletion of the headpiece domain of dematin. (*A Upper*)The genomic locus of mouse dematin gene and the targeting construct. Individual exons are shown by filled rectangles. (*Lower*)Schematic representation of the truncated dematin produced by the headpiece deletion. (*B*) Southern blot analysis of *Nco*I-digested genomic DNA isolated from wild-type (+/+) and targeted ES cells (+/−) by using the probe shown in *A*. (*C*) Tail genotyping of F_2 generation of wild-type (+/+), heterozygous (+/−), and homozygous (−/−) mice by using primers MD43 and MD32. (*D*) RT-PCR analysis of total RNA extracted from kidney and brain. Note the absence of 813-bp PCR product in the tissues of HPKO mice. (*E*) Coomassie blue-stained SDS/PAGE (10% gel) profile of erythrocyte ghosts prepared from wild-type (+/+) and dematin HPKO mice (−/−). Note that the protein 4.9 region that includes dematin, p55, and other polypeptides of unknown identity stains poorly with Coomassie blue and therefore both intact and truncated dematin polypeptides are barely visible. (*F*) Western blot analysis of erythrocyte ghosts prepared from wild-type (+/+) and dematin HPKO (−/−) mice by using a monoclonal antibody directed against the core domain of dematin. Note the absence of intact 48-kDa and 52-kDa polypeptides of dematin and a slightly faster mobility of the truncated dematin polypeptide in the dematin HPKO ghosts.

these cells. Therefore, our initial focus was to assess the impact of the headpiece domain deletion in mature erythrocytes. Biochemical analysis of erythrocyte membrane proteins by gel electrophoresis showed an apparently normal distribution of major membrane proteins (Fig. 1*E*). Spectrin-band 3, actin-protein 4.1, and protein 4.1-band 3 ratios remained essentially unaltered in the dematin HPKO ghosts as estimated by the scanning of Coomassie-stained polypeptides. Because it is difficult to visualize dematin by Coomassie staining, we used a monoclonal antibody directed against the N-terminal core domain of dematin to detect the presence of truncated dematin in HPKO ghosts (Fig. 1*F*). Western blotting shows the expected presence of 48-kDa and 52-kDa polypeptides of dematin in the wild type (+/+) ghosts, whereas a truncated polypeptide of ≈40 kDa was detected in the dematin HPKO ghosts (Fig. 1*F*). Because the 52-kDa subunit of dematin arises by the insertion of 22 aa within the headpiece domain of the 48-kDa subunit (10), the deletion of exons 11–15 eliminated the headpiece domains of both isoforms, thus producing a single truncated polypeptide encoding the N-terminal core domain of dematin (Fig. 1*F*).

Headpiece Null Mice Are Anemic and Display Mild Spherocytosis. Hematological evaluation of dematin HPKO mice provided evidence of mild anemia and compensated hemolysis (Table 1). Adult hematocrits are significantly reduced, reticulocyte counts are elevated, and RBCs are relatively smaller as evident by a significant decrease in the mean corpuscular volume. Phase contrast microscopy of unfixed RBCs partially exposed to hypotonic milieu shows evidence of spherocytic morphology in the dematin HPKO mice (Fig. 2). The scanning electron microscopy (SEM) further confirmed the spherocytic morphology of the headpiece null RBCs (Fig. 2). Moreover, the SEM established that the dematin HPKO erythrocytes are relatively smaller showing vesicular material budding off the surface membrane (Fig. 2). Together, these results demonstrate the existence of compensated anemia with microcytosis and spherocytosis caused by the deletion of the headpiece domain of dematin.

Table 1. Hematological parameters of wild-type and dematin headpiece null mice

	Wild type (+/+)	Dematin HPKO (−/−)
RBC, $\times 10^{12}$/liter	10.00 ± 0.51	9.60 ± 0.27
HCT, %	49.87 ± 3.32	43.12 ± 2.56
MCV, fl	50.32 ± 0.81	45.10 ± 1.0
MCHC, g/dl	25.75 ± 0.46	26.47 ± 0.20
HGB, g/dl	12.75 ± 0.86	11.62 ± 0.75
Retic, %	2.70 ± 0.25	5.05 ± 0.17

The values represent a mean of four adult (8–10 mo old) male mice. HPKO, headpiece knockout; RBC, red blood cells ($P = 0.213$); HCT, hematocrit ($P = 0.018$); MCV, mean corpuscular volume ($P = 0.000$); MCHC, mean corpuscular hemoglobin concentration ($P = 0.029$); HGB, hemoglobin ($P = 0.097$); Retic, reticulocytes ($P = 0.000$).

Headpiece Null Erythrocytes Are Fragile and Mechanically Unstable. Exposure to hypotonic stress by low ionic strength solutions was used to measure the osmotic fragility of dematin HPKO erythro-

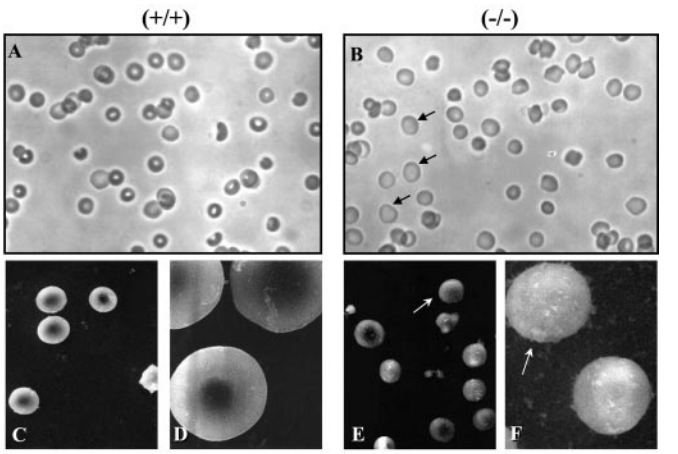

Fig. 2. Visualization of erythrocyte morphology. (*A*) The phase contrast micrograph of unfixed wild-type erythrocytes. (*C* and *D*) Scanning electron micrographs of the same cells at two magnifications. (*B*, *E*, and *F*) The same analysis for erythrocytes obtained from dematin HPKO mice. Note that the phase contract photographs shown in *A* and *B* were taken by incubation of erythrocytes in the 100.1-mOsm solution. Arrows in *B* indicate the abundance of spherocytic RBCs in the dematin HPKO mice. Microcytosis, as well as spherocytosis, is clearly visible by scanning electron microscopy. The dematin HPKO erythrocytes also display structures that resemble vesicles shedding from the cell surface. All studies were conducted on mice with mixed genetic background of 129/Sv and C57BL/6J.

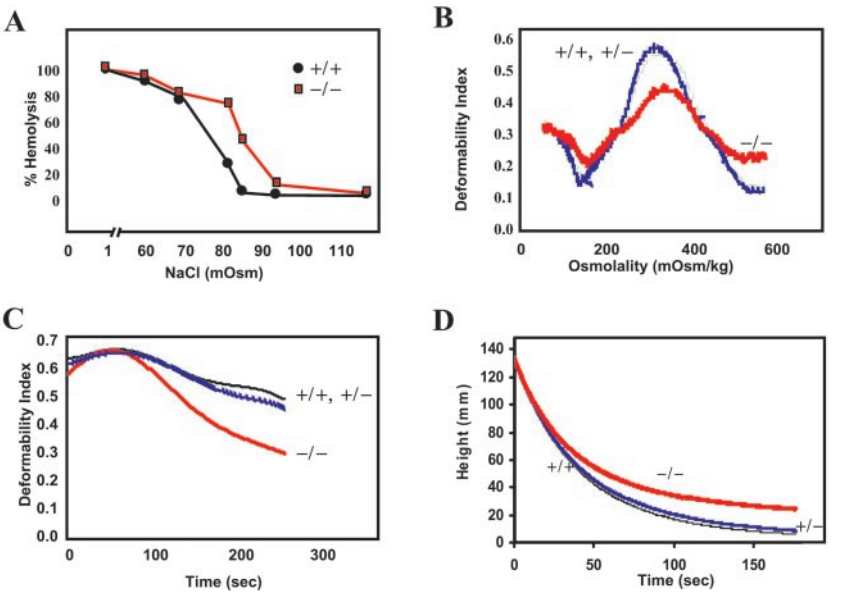

Fig. 3. Biophysical characterization of dematin HPKO erythrocytes. (*A*) Osmotic Fragility of wild-type (+/+) and HPKO (−/−) erythrocytes. Note that the headpiece null erythrocytes show a greater propensity of hemolysis under hypotonic conditions, as reflected by a right shift in the osmotic fragility curve. The values are: 1.5 mOsm, 99.96 ± 0. 05(+/+)and 99.99 ± 0.01 (−/−), $P = 0.476$; 62 mOsm, 91.40 ± 0.01 (+/+) and 93.50 ± 0.01 (−/−), $P = 0.000$; 69 mOsm, 77.83 ± 0.11 (+/+) and 81.80 ± 0.01 (−/−), $P = 0.000$; 83 mOsm, 27.20 ± 0.33 (+/+) and 77.49 ± 0.01 (−/−), $P = 0.000$; 85 mOsm, 5.39 ± 0.01 (+/+) and 45.89 ± 0.01 (−/−), $P = 0.000$; 93 mOsm, 4.00 ± 0.01 (+/+), 12.39 ± 0.01 (−/−), $P = 0.000$; 154 mOsm, 4.00 ± 0.01 (+/+) and 5.17 ± 0.06 (−/−), $P = 0.000$. (B) Osmotic gradient ektacytometry. Osmotic deformability was measured by subjecting the erythrocytes to moderate shear stress while increasing osmotic pressure. Deformability profiles generated by plotting osmolality against the deformability index (DI_{max}) are shown for the wild-type (+/+), heterozygous (+/−), and homozygous (−/−) erythrocytes. The data represent the outcome of three independent measurements carried out on 8-mo-old mice. The mean values of DI_{max} are: 0.55 ± 0.03 (+/+); 0.53 ± 0.02 (+/−); and 0.46 ± 0.02 (−/−). (*C*) Membrane fragmentation assay. Membrane stability of resealed erythrocyte membranes was examined under a constant high shear stress, and the rate of membrane fragmentation was measured by a decrease in the deformability index with time. Note that the dematin HPKO (−/−) erythrocyte membranes fragmented more rapidly than the wild-type membranes. The mean values of half-time membrane fragmentation are: 176 ± 4.0 s (+/+), 175 ± 7.0 s (+/−), 140 ± 3.0 s (−/−). (*D*) Erythrocyte filterability was evaluated by allowing RBCs at 0.1% hematocrit to flow through a 4.6-μm pore-sized nickel mesh filter. The height of the erythrocyte suspension was recorded as a function of time as the cells were forced by hydrostatic pressure through the filter. All measurements were performed on freshly collected blood stored in excess glucose for a few hours. The results reflect the outcome of experiments conducted on six mice of 8 mo old for each measurement.

cytes (Fig. 3*A*). Erythrocytes from dematin HPKO mice were significantly more susceptible to hemolysis, with 50% of the cells lysing at a salt concentration significantly higher (≈85 mOsm) than that causing hemolysis of wild-type erythrocytes (≈75 mOsm). Osmotic gradient ektacytometry measurements indicate a marked reduction in the maximum value of the deformability index (DI_{max}) of dematin HPKO erythrocytes (Fig. 3*B*). More importantly, the rate of erythrocyte membrane fragmentation on exposure to a constant high shear stress revealed a significantly shorter halftime for fragmentation of headpiece null erythrocytes as compared with cells from the wild-type and heterozygous littermates (Fig. 3*C*). Finally, the filterability of dematin HPKO erythrocytes through a 4.6-μm nickel mesh filter was ≈10% lower than that of wild-type erythrocytes (Fig. 3*D*). Together, these results demonstrate that the plasma membrane of dematin HPKO erythrocytes is markedly less stable and fragments faster than normal erythrocytes.

Headpiece Domain Is Essential for the Retention of Spectrin-Actin Complex in the Membrane Skeleton. To further investigate the molecular basis of membrane instability in dematin HPKO erythrocytes, we first examined the effect of the headpiece domain deletion on the constituents of erythrocyte membrane skeletons. Detergent-extracted cytoskeletons (Triton shells) were prepared from ghosts in the presence of increasing salt concentrations (Fig. 4*A*). Quantification by gel densitometry revealed a significant reduction in the amount of actin associated with the membrane skeletons of dematin HPKO ghosts (Fig. 4*A*). Membrane skeletons prepared in the presence of Triton X-100 alone retain a significant amount of band 3, which served as an internal control to quantify diminished amount of actin. The actin to band 3 ratio was decreased by ≈35% in dematin HPKO erythrocyte membrane skeletons (Fig. 4*A*, lanes 1 and 2). When membrane skeletons are prepared in the presence of 0.5 M KCl, where no band 3 is retained, the amount of spectrin and actin was reduced by ≈40% in the dematin HPKO skeletons (Fig. 4*A*, lanes 5 and 6). These results suggest that the deletion of the headpiece domain of dematin weakens the association of spectrin–actin complex to the erythrocyte plasma membrane. To extend this observation further, we partially extracted spectrin–actin complexes from ghosts by the treatment with cold hypotonic buffer solution (Fig. 4*B*). Indeed, the headpiece null IOVs lost significantly higher amount of spectrin and actin than that of wild-type IOVs (Fig. 4*B*, lane 4). The α-spectrin to band 3 ratio was reduced by ≈60% in the headpiece null IOVs (Fig. 4*B*, lanes 3 and 4). It is noteworthy here that the hypotonic buffer extraction at 37°C did not permit quantification of weakened interactions because of

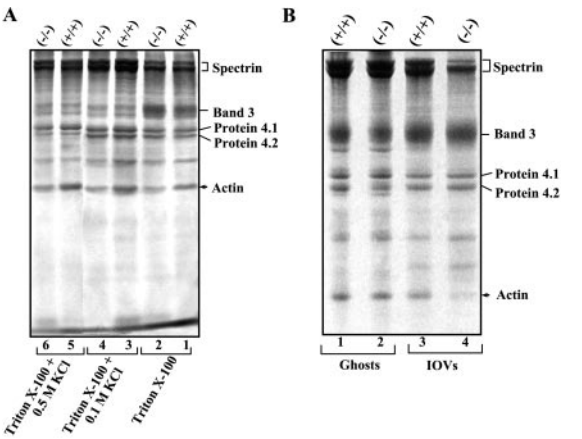

Fig. 4. Effect of dematin headpiece deletion on the association of spectrin and actin to the erythrocyte plasma membrane. (*A*) RBC ghosts were solubilized in 1% Triton X-100 with increasing concentration of KCl, which results in the extraction of band 3 and other transmembrane proteins progressively. High-speed pellets (Triton shells) were analyzed by 10% SDS/PAGE. Note that significantly higher amount of actin (indicated by an arrowhead) was lost from the HPKO skeletons (see lanes 2, 4, and 6). The reduced amount of actin in lane 2, relative to lane 1, was quantified by determining the ratio of actin to band 3 as described in the text. All experiments were repeated at least three times with similar results. (*B*) Dissociation of spectrin–actin complex from ghosts by low ionic strength solution. IOVs were prepared by incubation of ghosts in the low ionic strength buffer on ice. Note that significantly higher amount of spectrin–actin complex was dissociated from the headpiece null IOVs (lane 4) whereas the relative amount of other major proteins remains unaltered. All experiments were repeated at least three times with similar results.

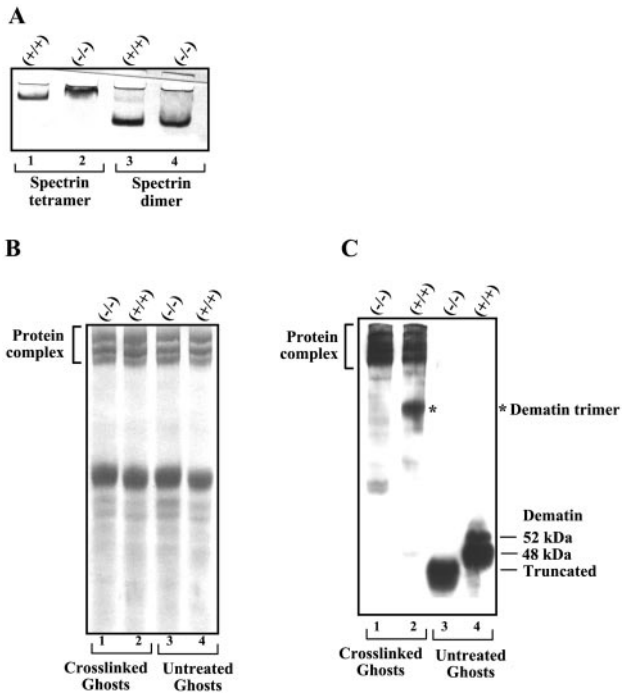

Fig. 5. Biochemical characterization of dematin HPKO ghosts. (*A*) Spectrin dimer-tetramer equilibrium analysis. Spectrin was extracted at 0°C and analyzed by 4% nondenaturing PAGE. Note that the amount of spectrin tetramer extracted at 0°C and its conversion to dimer remained unaltered by the deletion of the headpiece domain. (*B*) Chemical crosslinking of RBC ghosts. Copper sulfate and *O*-phenanthroline crosslinked proteins were analyzed by 5.6% Fairbanks gel system without the reducing agent. Coomassie blue-stained polyacrylamide gel shows the region of higher m.w. complex (lanes 1 and 2) in both wild-type and HPKO ghosts. (*C*) The gel shown in *B* was transferred to the nitrocellulose membrane and Western blotted by using a monoclonal antibody against the core domain of dematin. The high m.w. complex was detected in wild-type as well as HPKO ghosts, demonstrating the participation of both intact and truncated dematin in the complex formation. It is noteworthy that the high m.w. complex containing dematin migrates as a diffuse band in the mouse ghosts. This result is in contrast to a well-defined high m.w. complex observed in human ghosts (data not shown). Interestingly, the formation of sulfhydryl crosslinked dematin trimer (shown by asterisk in lane 2) was eliminated by the deletion of the headpiece domain.

the complete removal of the spectrin–actin complex from wild-type as well as dematin HPKO ghosts (data not shown). Next, we examined whether alterations in the self-association of spectrin might also contribute to the observed membrane instability in dematin HPKO erythrocytes. As shown in Fig. 5*A*, the same amount of tetrameric spectrin was recovered from wild-type and dematin HPKO ghosts. Moreover, no differences were observed in the dimer-tetramer equilibrium of spectrin *in vitro* (Fig. 5*A*). Together, these results indicate that the deletion of the headpiece domain of dematin results in the destabilization of the spectrin–actin association with the erythrocyte plasma membrane without any influence on the self-association of spectrin.

Headpiece Domain Is Required for the Assembly of Dematin Trimer. Previous studies have established that dematin forms a trimer in solution (8, 11). Based on sequence of 48-kDa and 52-kDa subunits, a model has been proposed where the headpiece domain plays a critical role in the assembly of dematin trimer (10). We used a well-established chemical crosslinking approach to test whether the deletion of dematin headpiece domain disrupts the formation of trimer and influences dematin's ability to interact with its surrounding cytoskeletal components (11, 24). Ghosts were subjected to copper-phenanthroline-mediated oxidation, a stress that is known to promote formation of the crosslinked protein complexes (11, 25), and analyzed crosslinked products by gel electrophoresis in the absence of reducing power (Fig. 5*B*, lanes 1 and 2). The formation of dematin trimer (≈148 kDa) in the wild-type ghosts was confirmed by Western blotting using a monoclonal antibody specific for the core domain of dematin (Fig. 5*C*, asterisk in lane 2). In contrast, the formation of sulfhydryl-linked trimer was completely eliminated by the deletion of dematin headpiece domain (Fig. 5*C*, lane 1), indicating an essential requirement of this domain in trimer formation. Moreover, the chemical crosslinking approach allowed us to examine whether the crosslinking of dematin into the high m.w. complex is altered in the dematin HPKO erythrocytes (24, 25). The formation of the high m.w. complex, containing dematin, β spectrin, and other unknown polypeptides remained unaltered by the deletion of the headpiece domain, indicating that the N-terminal core domain of dematin is sufficient to mediate crosslinking of dematin with other proteins under these conditions (Fig. 5*C*, lanes 1 and 2). Together, these results indicate that the deletion of the headpiece domain prevents sulfhydryl-linked assembly of the dematin trimer but does not affect the crosslinking of dematin to other proteins in the plasma membrane.

Discussion

Spectrin is the most abundant protein in the membrane skeleton and plays a critical role in the maintenance of erythrocyte shape and membrane properties (1, 2). The mechanism by which the head region of spectrin binds to the membrane via ankyrin and band 3 has been relatively well characterized (1). But the mechanism by which the tail end of spectrin is anchored to the plasma membrane is not completely understood. The tail end region of spectrin that contains actin protofilaments is often referred to as "spectrin–actin junctions" or simply "junctional complexes" (26). Actin, protein 4.1, dematin, and adducin have been directly visualized as components of junctional complexes (27). Other proteins likely to be located at junctional complexes include tropomyosin, tropomodulin, and calmodulin (26, 28). Because the core of the RBC membrane skeleton consists of spectrin, actin, protein 4.1, and dematin, an understanding of dematin function remains a matter of considerable interest. There are perhaps three main reasons why the physiological function of dematin remains a mystery. First, the dematin polypeptides stain poorly with the Coomassie blue and therefore often escape the visual diagnostics of Coomassie-stained polyacrylamide gels. Second, the powerful approach of correlating defects in RBC membrane structure with mutations in membrane proteins in patients with hemolytic anemia has failed to identify abnormalities in the dematin gene. Finally, with the exception of F-actin, dematin protein does not appear to associate with other components that are especially rich in the RBC membrane.

Our previous biochemical and genetic characterization of dematin has shown that both 48- and 52-kDa subunits of dematin contain a C-terminal headpiece domain that is homologous to the headpiece domain of villin (10, 23). The 383-residue, 48-kDa subunit consists of an N-terminal core domain that includes a proline-rich motif (PEST), a polyacidic motif, and a C-terminal 75-residue headpiece domain (23). The 52-kDa subunit arises by an insertion of exon 13 that contributes 22 residues within the headpiece domain of 48-kDa subunit (10, 15). The 22-residue insertion of 52-kDa subunit includes a protein 4.2-homology motif, an ATP-binding site, and a cysteine residue that is believed to participate in the assembly of sulfhydryl-linked trimers of dematin (10, 29). The headpiece domain is a compact, protease-resistant module that contains an actin-binding site and a cAMP-kinase phosphorylation site at serine-384 (23). Phosphorylation of serine-384 by an endogenous cAMP-kinase abolishes the actin-bundling activity of dematin *in vitro* (8, 9). We reasoned that the deletion of the headpiece domain might provide novel insights into the physiological function of dematin *in vivo*. The targeting construct used here was engineered to delete exons 11–15 that encode the headpiece domain of

dematin (Fig. 1*A*). Indeed, the Western blotting results confirm that our strategy deleted the headpiece domains of both 48-kDa and 52-kDa subunits of dematin (Fig. 1*F*). These results also demonstrate that the core domain of dematin could still be expressed although the amount of truncated protein is reduced by ≈50% in the headpiece null erythrocyte ghosts (Fig. 1*F*).

Dematin is a potent actin-bundling protein *in vitro*. With the notion that the actin bundles do not exist in mature RBCs, the presence of dematin in erythrocytes remains a puzzle. Hematological data shown in Table 1 demonstrate that the deletion of the headpiece domain of dematin results in compensated anemia, microcytosis, and spherocytosis (Fig. 2). More importantly, the headpiece null RBCs are osmotically fragile, and ektacytometry results show a marked reduction in the maximum deformability index consistent with the loss of surface area (Fig. 3 *A* and *B*). Moreover, the propensity of fragmentation of resealed erythrocyte membranes under stress is significantly greater (Fig. 3*C*), further underscoring the importance of the headpiece domain in the maintenance of membrane mechanical properties. Mechanistically, the deleterious effects of the headpiece mutation appear to result in the selective loss of spectrin and actin from RBC membrane skeletons and vesicles without any discernible alterations of other major proteins (Fig. 4). It is noteworthy that the absence of the headpiece domain does not influence the dimer-tetramer equilibrium of spectrin (Fig. 5*A*), which is consistent with our model supporting a role of dematin at the tail end of spectrin where actin oligomers crosslink spectrin into the membrane skeleton.

The generation of mutant mice selectively lacking the headpiece domain of dematin provided a unique opportunity to test our model that the headpiece domain is essential for the assembly of disulfide-linked trimer (10). Notwithstanding the importance of the headpiece domain in dematin trimer formation (Fig. 5), the present study does not address the issue of whether trimer formation is necessary for the retention of spectrin–actin complex in the membrane skeleton. The precise mechanism by which deletion of the headpiece domain weakens the spectrin–actin linkage in the membrane skeleton remains to be elucidated. The retention of the core domain in RBC ghosts implies the existence of membrane-binding sites in dematin that are independent of the headpiece domain. Consistent with this notion is the observation that the bulk of dematin remains associated with the membrane vesicles when spectrin–actin complex is removed by low ionic strength extraction (30). Moreover, the chemical crosslinking data show that the core domain of dematin is also incorporated into sulfhydryl-crosslinked protein complex that contains β-spectrin (Fig. 5). Because dematin does not raise the critical actin concentration, and therefore is unlikely to cap the barbed ends of the actin filaments (11), we propose a model where the N-terminal core domain of dematin binds to spectrin and an as yet unknown membrane protein providing a molecular bridge between the spectrin–actin complex and the RBC plasma membrane. The deletion of the headpiece domain uncouples this linkage, thus destabilizing the structural integrity of the erythrocyte membrane *in vivo*.

There are several parallels between the properties of dematin and adducin in the erythrocyte membrane, which are both located at the spectrin–actin junctions (27). Adducin, consisting of α and β subunits, promotes the association of spectrin with F-actin, bundles actin filaments, and caps barbed ends of actin filaments *in vitro* (31) (32–34). Surprisingly, recent generation of β adducin null mice, which also lack ≈80% of α adducin, revealed a nearly normal content of spectrin and actin in the erythrocyte ghosts (35, 36). The retention of spectrin–actin complex in the membrane skeletons of β adducin null RBCs has not been examined as yet. By crossbreeding dematin headpiece null and β adducin null mice in the future, it would be feasible to determine whether dematin and adducin perform any redundant functions *in vivo*. Intriguingly, the loss of either β adducin or dematin headpiece domain results in comparable levels of osmotic fragility of RBCs and spherocytosis, necessitating a closer scrutiny of these proteins in hemolytic anemia patients with unknown etiology.

The 75-residue headpiece domain of dematin is homologous to the headpiece domain of villin, an actin-binding protein of the brush border cytoskeleton (23). *In vitro*, the headpiece domain of villin plays a crucial role in actin-bundling events and morphogenesis of microvilli. Recent evidence from villin null mice suggests that villin plays a minor or redundant role in the development of microvilli in absorptive tissues (37, 38). Interestingly, further characterization of villin null mice revealed that, whereas villin is not necessary for bundling actin filaments *in vivo*, it plays a role in the reorganization of actin filaments in response to various stimuli (38). These observations raise the possibility that loss of villin may be compensated by dematin and/or other headpiece-containing proteins, such as supervillin and limatin. Clearly, answers to some of these questions might require deletion of the full-length dematin to gain further insights into the physiological function(s) of dematin in erythroid as well as non-erythroid cells. Indeed, an initial pathological examination of the dematin headpiece null mice revealed evidence of lymphoid hyperplasia in the spleen and lymphoid infiltration in various organs, necessitating a future investigation of the role of dematin in lymphocyte physiology.

We thank Dr. Toshi Hanada of St. Elizabeth's Medical Center for his valuable advice and many helpful discussions during the course of these studies. We are grateful to Mr. Gary Sclar for help with the microinjection experiments, Ms. Donna Marie-Mironchuk for the artwork, and Drs. M. Hanspal and S. Oh for critically reviewing the manuscript. This work was supported by National Institutes of Health Grants HL 51445 and HL 60755.

1. Lux, S. E. & Palek, J. (1995) in *Blood: Principles and Practice of Hematology*, eds. Handin, R. I., Lux, S. E. & Stossel, T. P. (Lippincott, Philadelphia), pp. 1701–1718.
2. Elgsaeter, A., Stokke, B. T., Mikkelsen, A. & Branton, D. (1986) *Science* **234,** 1217–1223.
3. Sheetz, M. P. (1979) *Biochim. Biophys. Acta* **557,** 122–134.
4. Luna, E. J. & Hitt, A. L. (1992) *Science* **258,** 955–964.
5. Bennett, V. (1989) *Biochim. Biophys. Acta* **988,** 107–121.
6. Holdstock, S. J. & Ralston, G. B. (1983) *Biochim. Biophys. Acta* **736,** 214–219.
7. Faquin, W. C., Chahwala, S. B., Cantley, L. C. & Branton, D. (1986) *Biochim. Biophys. Acta* **887,** 142–149.
8. Chishti, A., Faquin, W., Wu, C. C. & Branton, D. (1989) *J. Biol. Chem.* **264,** 8985–8991.
9. Chishti, A., Levin, A. & Branton, D. (1988) *Nature (London)* **334,** 718–721.
10. Azim, A. C., Knoll, J. H., Beggs, A. H. & Chishti, A. H. (1995) *J. Biol. Chem.* **270,** 17407–17413.
11. Siegel, D. L. & Branton, D. (1985) *J. Cell Biol.* **100,** 775–785.
12. Byers, T. J. & Branton, D. (1985) *Proc. Natl. Acad. Sci. USA* **82,** 6153–6157.
13. Shen, B. W., Josephs, R. & Steck, T. L. (1986) *J. Cell Biol.* **102,** 997–1006.
14. Friederich, E., Vancompernolle, K., Louvard, D. & Vandekerckhove, J. (1999) *J. Biol. Chem.* **274,** 26751–26760.
15. Kim, A. C., Azim, A. C. & Chishti, A. H. (1998) *Biochim. Biophys. Acta* **1398,** 382–386.
16. Azim, A. C., Kim, A. C., Lutchman, M., Andrabi, S., Peters, L. L. & Chishti, A. H. (1999) *Mamm. Genome* **10,** 1026–1029.
17. Clark, M. R., Mohandas, N. & Shohet, S. B. (1983) *Blood* **61,** 899–910.
18. Johnson, R. M. (1989) *Methods Enzymol.* **173,** 35–54.
19. Mohandas, N., Clark, M. R., Health, B. P., Rossi, M., Wolfe, L. C., Lux, S. E. & Shohet, S. B. (1982) *Blood* **59,** 768–774.
20. Arai, K., Iino, M., Shio, H. & Uyesaka, N. (1990) *Biorheology* **27,** 47–65.
21. Liu, S. C., Palek, J., Prchal, J. & Castleberry, R. P. (1981) *J. Clin. Invest.* **68,** 597–605.
22. Fairbanks, G., Steck, T. L. & Wallach, D. F. (1971) *Biochemistry* **10,** 2606–2617.
23. Rana, A. P., Ruff, P., Maalouf, G. J., Speicher, D. W. & Chishti, A. H. (1993) *Proc. Natl. Acad. Sci. USA* **90,** 6651–6655.
24. Liu, S. C., Fairbanks, G. & Palek, J. (1977) *Biochemistry* **16,** 4066–4074.
25. Liu, S. C. & Palek, J. (1979) *J. Supramol. Struct.* **10,** 97–109.
26. Gilligan, D. M. & Bennett, V. (1993) *Semin. Hematol.* **30,** 74–83.
27. Derick, L. H., Liu, S. C., Chishti, A. H. & Palek, J. (1992) *Eur. J. Cell Biol.* **57,** 317–320.
28. Bennett, V. & Gilligan, D. M. (1993) *Annu. Rev. Cell Biol.* **9,** 27–66.
29. Azim, A. C., Marfatia, S. M., Korsgren, C., Dotimas, E., Cohen, C. M. & Chishti, A. H. (1996) *Biochemistry* **35,** 3001–3006.
30. Steck, T. L. (1974) *J. Cell Biol.* **62,** 1–19.
31. Mische, S. M., Mooseker, M. S. & Morrow, J. S. (1987) *J. Cell Biol.* **105,** 2837–2845.
32. Gardner, K. & Bennett, V. (1987) *Nature (London)* **328,** 359–362.
33. Joshi, R., Gilligan, D. M., Otto, E., McLaughlin, T. & Bennett, V. (1991) *J. Cell Biol.* **115,** 665–675.
34. Kuhlman, P. A., Hughes, C. A., Bennett, V. & Fowler, V. M. (1996) *J. Biol. Chem.* **271,** 7986–7991.
35. Gilligan, D. M., Lozovatsky, L., Gwynn, B., Brugnara, C., Mohandas, N. & Peters, L. L. (1999) *Proc. Natl. Acad. Sci. USA* **96,** 10717–10722.
36. Muro, A. F., Marro, M. L., Gajovic, S., Porro, F., Luzzatto, L. & Baralle, F. E. (2000) *Blood* **95,** 3978–3985.
37. Pinson, K. I., Dunbar, L., Samuelson, L. & Gumucio, D. L. (1998) *Dev. Dyn.* **211,** 109–121.
38. Ferrary, E., Cohen-Tannoudji, M., Pehau-Arnaudet, G., Lapillonne, A., Athman, R., Ruiz, T., Boulouha, L., El Marjou, F., Doye, A., Fontaine, J. *et al.* (1999) *J. Cell Biol.* **146,** 819–830.